Recovery of Antimony: A Laboratory Study on the Thermal Decomposition and Carbothermal Reduction of Sb(III), Bi(III), Zn(II) Oxides, and

Journal of Sustainable Metallurgy (2018) 4:194–204
https://doi.org/10.1007/s40831-017-0156-y

INNOVATIONS IN WEEE RECYCLING

Recovery of Antimony: A Laboratory Study on the Thermal Decomposition and Carbothermal Reduction of Sb(III), Bi(III), Zn(II) Oxides, and Antimony Compounds from Metal Oxide Varistors

Toni Karlsson[1] · Christer Forsgren[2] · Britt-Marie Steenari[1]

Published online: 11 January 2018

Abstract
As antimony is typically present in industrial and commercial products only in small amounts, the concentration of antimony in waste types is low and a limited amount of antimony is currently recycled. One product relatively rich in antimony is the metal oxide varistor (MOV) used for overvoltage protection in electric circuits. To increase the antimony concentration, the MOV was pulverized (< 65 μm) and leached, resulting in an insoluble MOV residue containing 186 ± 2 mg/g of antimony. This work investigates the thermal decomposition and carbothermal reduction of pure metal oxides (Sb_2O_3, Bi_2O_3, and ZnO) and MOV residue. Thermogravimetric (TG) analysis was used in order to propose a temperature range in which it is possible to separate antimony oxide from the MOV residue. TG results indicate that during thermal decomposition of pure metal oxides, sublimated antimony oxide can be recovered at 650 °C, leaving Bi_2O_3 and ZnO unreacted. The addition of carbon caused mainly volatilization, with some reduction, of Sb_2O_3 and reduction of Bi_2O_3 to occur at nearly the same temperature, approximately 600 °C. However, volatilization of Bi was not troublesome below 800 °C due to slow kinetics. Thermal decomposition of antimony from the MOV residue was not possible in the temperature range studied (< 1000 °C), while carbothermal reduction to the MOV residue revealed antimony volatilization occurred near 800 °C.

Keywords Antimony · Varistor · Recycling · Bismuth · Carbothermal reduction

Introduction

Within the European Union (EU), the major use of antimony is in the form of antimony oxide (Sb_2O_3) as a flame retardant in plastics and textiles [1]. Worldwide, metallic antimony is used in lead–acid batteries and in ammunition. Other uses are as a vulcanizing agent in rubber production, as a polymerization catalyst in the production of plastics and as a pigment in ceramic and glass [2].

The EU is dependent entirely on imports of antimony [1], and in 2015 the United States (US) imported 23,600 metric tons of antimony for industrial consumption [3]. The antimony used in the US was imported mainly from the People's Republic of China (63%), Bolivia (8%), Belgium (7%), and Thailand (6%). The People's Republic of China is currently the leading producer of antimony with its government classifying antimony as a strategic material and controlling annual production quotas [3]. Currently, there are known to be 1.5 million tons of antimony reserves worldwide. At current mining rates, known antimony reserves will be depleted by 2027 [2].

From a recycling perspective, hardly any antimony is recycled. This is mostly because its applications are highly dispersive and collection is difficult [4]. Conventional recycling routes are typically not applicable to metals such as antimony [5] if no pretreatment step(s) to create concentrates are taken. Antimony is used extensively as a flame retardant, thus it is found in very low concentrations in plastics and textiles, making it impossible to design a

The contributing editor for this article was Bernd Friedrich.

✉ Toni Karlsson
tonig@chalmers.se

[1] Industrial Materials Recycling, Department of Chemistry and Chemical Engineering, Chalmers University of Technology, Kemivägen 4, 412 96 Gothenburg, Sweden

[2] Stena Metall AB, Fiskhamnsgatan 8D, Box 4088, 400 40 Gothenburg, Sweden

recycling route from this waste stream [5] unless pretreatment steps are taken.

There are several waste streams from which antimony can be recovered; one success story is recycling antimony from lead–acid batteries. In the lead–acid battery, antimony is used in lead–antimony alloy plates in order to make this alloy harder. The concentration of antimony in lead–acid batteries has been declining due to advances in battery technology; however, the use of lead–acid batteries continues to increase. Nearly 85% of lead–acid batteries are recycled in the United States due to implementation of a policy restricting battery disposal in landfills and the availability of collection sites. Lead–acid batteries are the main source of secondary antimony. Antimony is recovered from the secondary lead smelter as an antimonial lead mixture and put back into production of new batteries [2]. In 2015, the US recycled 3850 metric tons of antimony [3].

Antimony recovery from municipal solid waste (MSW) incineration ash is another possible source of secondary antimony. MSW contains items having antimony thinly dispersed within them. Incineration can be thought of as a type of pretreatment step. Household wastes such as textiles contain 25.9 mg/kg antimony while plastics and rubber contain 12.9 and 8.4 mg/kg, respectively [6]. Items such as curtains contain larger concentrations of antimony and things like wood contain much less antimony. It is estimated that the average antimony concentration in MSW is around 10–60 mg/kg [7, 8]. After incineration, the concentration of antimony in fly ash varies depending on the starting material and incineration conditions, but it has been shown to be less than < 2000 mg Sb/kg dry ash [9–11].

In ammunition, lead is alloyed with antimony (2–5 wt%) [12]; therefore, the accumulation of ammunition fired at shooting ranges could be a potential source of secondary antimony. In a study by Johnson et al. [12], the antimony concentration in shooting range soil samples was shown to be 35–17,500 mg/kg.

In some cases, antimony is added to ceramics as a pigment and it can also be used to enhance specific characteristics. Antimony oxide is used in a type of ceramic known as the metal oxide varistor (MOV), which is a zinc oxide-based ceramic semiconducting device with a high degree of non-linear current–voltage characteristics. The main application of zinc oxide varistors is in circuits for overvoltage protection. An example of its use is in surge arrestors or lightening protectors on power lines [13]. Zinc oxide varistors are commonly referred to as MOVs due to the presence of zinc, bismuth, antimony, cobalt, manganese, and nickel oxides in addition to other metal oxides used in low amounts. It is not known how much antimony is available from varistors worldwide. However, used varistors could be a good source of recovered antimony since their Sb concentration is relatively high. In Sweden, it has been estimated that from 2009 to 2013 just over 520 metric tons of varistors were produced [14]. If secondary antimony oxide could be recovered, 23 metric tons of antimony would be available for reuse.

The MOV under investigation in this study is composed of sintered zinc oxide (88.2 wt%), antimony trioxide (4.4 wt%), bismuth trioxide (5.1 wt%), cobalt trioxide (< 1 wt%), nickel oxide (< 1 wt%), and manganese carbonate (< 1 wt%) [15, 16]. Antimony oxide is used in the varistor to reduce the average size of the ZnO grain [17–19]. The microstructure of the MOV contains three phases, the most dominant phase being that of the zinc oxide grains. A bismuth-rich phase encompasses the zinc oxide grains and the antimony-rich phase is located within the bismuth oxide phase. XRD analysis has shown antimony compounds such as spinel ($Zn_7Sb_2O_{12}$, $Zn_{2.33}Sb_{0.67}O_4$) and pyrochlore ($Zn_2Bi_3Sb_3O_{14}$) [16–18] to be present in the MOV.

It has previously been shown by Gutknecht et al. [15] that a pretreatment step such as acid leaching of the pulverized MOV material solubilizes the zinc oxide phase while leaving the antimony and bismuth-rich phases concentrated in the insoluble residue. Before leaching, the amount of antimony in the MOV was 35 mg per gram MOV; after leaching there were 186 mg of antimony per gram residue, i.e., leaching as a pretreatment step increased the antimony concentration over 5 times.

Antimony is typically classified as a volatile heavy metal, and low-grade ores are commonly produced by pyrometallurgical methods [20]. Industrially, reduction of antimony oxide to metallic antimony is achieved by heating and the addition of carbon in a reverberatory furnace. Volatilization of antimony can be reduced by the addition of an alkaline flux but it cannot be eliminated [20] and volatilized antimony oxide is recovered in flues, condensing pipes, bag houses, precipitators, or a combination [21]. The volatile nature of antimony oxide can be utilized in designing a high-temperature method for separating gaseous antimony oxide from the matrix of the MOV leaching residue. Since the MOV residue is composed mainly of compounds containing zinc–antimony–oxygen, it was thought that the addition of carbon would help lower the Sb_2O_3 volatilization temperature by decomposition of the spinel/pyrochlore compounds.

Materials and Methods

This work used thermogravimetric analysis (TGA) to investigate the amount and rate of weight change of simple metal oxides and MOV residue as a function of temperature in inert and reducing conditions. Simple metal oxides

were used as a reference to help predict the behavior of sintered metal oxide compounds ($Zn_7Sb_2O_{12}$, $Zn_{2.33}Sb_{0.67}O_4$, and $Zn_2Bi_3Sb_3O_{14}$) present in the MOV residue. Carbothermal reduction experiments were done to observe if the volatilization temperature can be lowered compared to thermal decomposition from heat treatment. From TG results, a suitable high-temperature separation process can be proposed for the recovery of volatilized antimony oxide from the MOV residue.

MOV Pretreatment

A pulverized (crushed to a particle size < 65 μm) MOV was leached at pH 4 using H_2SO_4. Sulfuric acid was used because the leachate, once separated from the insoluble residue, could be sold to a zinc electrowinning facility for the production of secondary metallic zinc. It was demonstrated that the leachate contained low concentrations of cobalt and nickel, which can be removed by cementation [16], as well as some manganese. In previous work, the concentration of zinc in the leachate was shown to be 1 mol/l but can be increased to suit the needs of the electrowinning facility [16]. Other mineral acids as well as organic acids could also have been used for zinc leaching [15], but from those leachates, zinc or zinc oxide would have been recovered by precipitation or solvent extraction. The process for pretreatment of the MOV is described in detail in previous work by Gutknecht et al. [16].

In order to determine the composition of the insoluble MOV residue, a sample was dissolved in concentrated hydrochloric acid (37%) for 24 h while being continuously stirred using a magnetic stir bar. The solution was blue–green but transparent after dissolution. HCl was used due to the reported solubility of antimony compounds in concentrated hydrochloric media [22]. Elemental analysis using inductive coupled plasma with optical emission spectrometric detection (ICP-OES) (iCAP 6500, Thermo Fischer) yielded the results shown Table 1. The concentrations shown in Table 1 are given as milligrams of metal per gram of MOV residue. Metals account for approximately 85% of the MOV residue while it is assumed oxygen accounts for the remaining 15%. It was reasonable to assume oxygen makes up the remaining 15% due to X-ray analysis and compound identification.

Table 1 Composition of the leaching residue given in mg/g

Metal	mg/g
Bi	247 ± 2
Co	11.8 ± 0.1
Mn	14.7 ± 0.1
Ni	25.9 ± 0.1
Sb	186 ± 2
Zn	360 ± 1
Total	845 ± 5

Starting materials were analyzed for purity and identification of crystalline compounds present in the samples using an X-ray diffractometer (Bruker 2D Phaser) equipped with a characteristic Cu radiation source and a scintillation detector. Compound identification was made by comparisons with standards in the Joint Committee of Powder Diffraction Standards database [23]. The appearance and composition of the dried residue was analyzed with a SEM: A FEI Quanta 200 environmental SEM equipped with Oxford Inca energy dispersive X-ray detector (EDX) system. Imaging was done with accelerating voltages between 10 and 20 kV to obtain qualitative data about the elements present and to determine the occurrence and distribution of the components.

Materials Used

Pure samples of Sb_2O_3 (Sigma Aldrich, 99.9%), Bi_2O_3 (Sigma Aldrich, 99.9%), and ZnO (Sigma Aldrich, $\geq$ 99.9%) were used to determine the temperature range needed to thermally decompose or reduce the pure oxides. Because X-ray powder diffraction patterns showed that the metal oxides supplied were pure, the oxides were used without any further purification.

The pure metal oxides were a less complex system than the MOV residue and they provided a good fundamental understanding of the behavior of the metal oxides prior to analysis of the more complex MOV residue system. Pure metal oxides were also used as quasi-method checks, since their thermal properties are well documented in literature. The MOV residue was prepared as previously described having the metal concentration as shown in Table 1. The microstructure of the MOV residue is shown in Fig. 1. There are two main phases in the MOV residue: the Bi_2O_3 phase and the antimony-rich phase containing compounds such as spinel (α-$Zn_7Sb_2O_{12}$, β-$Zn_{2.33}Sb_{0.67}O_4$) and pyrochlore ($Zn_2Bi_3Sb_3O_{14}$).

In the MOV residue, it was seen that Bi_2O_3 encompassed the Sb-rich material as shown in Fig. 1. Cobalt, manganese, and nickel are also present in the MOV in much lower concentrations, most likely substituted into the spinel lattice. XRD analysis of the MOV residue supports this conclusion where peaks were seen for Zn–Co–Sb–O and Zn–Ni–Sb–O compounds. XRD also showed the presence of Bi_2O_3, $Zn_7Sb_2O_{12}$, and $Zn_2Bi_3Sb_3O_{14}$.

Thermogravimetric Experiments

HSC Chemistry 9 software was used for thermodynamic calculations regarding the equilibrium composition and Ellingham diagram reactions over a temperature range

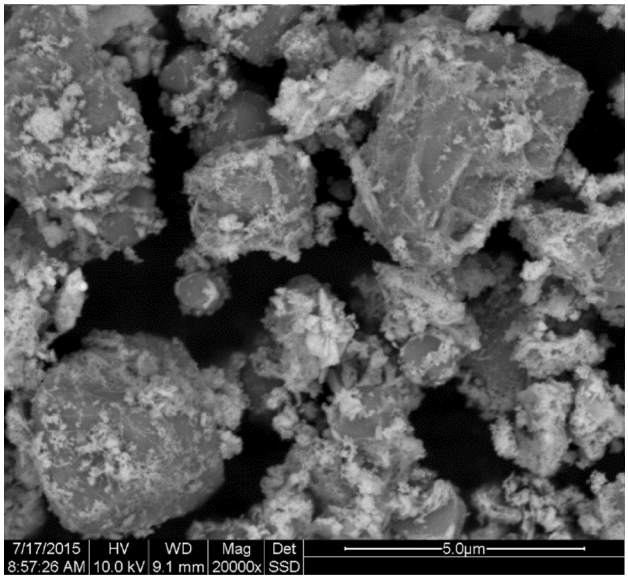

Fig. 1 SEM micrograph of MOV residue

from 100 to 1000 °C in a closed system. Thermogravimetric (TG) experiments were carried out on the Sb_2O_3, Bi_2O_3, ZnO, and MOV residue using a TA Instruments TGA Q500 equipped with a single control/sample thermocouple positioned immediately adjacent to the sample. The TGA had a quartz-lined furnace with a nitrogen sample and balance purge gas. Use of the TG was limited to temperatures below 1000 °C. Typical operating parameters for TG are given in Table 2. Thermolysis curves are displayed as % mass loss (m) versus temperature or when needed the derivative ($\Delta m/\Delta t$) showing the rate of weight loss as a function of temperature. The TG was calibrated with five high-purity standards using their Curie temperature and peak inflection point as the calibration temperature.

Two general types of experiments were performed: (1) thermal decomposition where the metal oxides as well as MOV residue were heated in a nitrogen atmosphere and (2) carbothermal reduction where charcoal was added to the metal oxides and MOV residue. It has been proven to work in zinc production [24] but the effect on the oxides of antimony and bismuth as well as the MOV residue is not well known.

For carbothermal reduction experiments, activated charcoal (DARCO®, − 100 mesh) was mixed with the metal oxides and the MOV residue at multiple C/O molar ratios. Homogenization was done using a mortar and pestle. The C/O ratio for the MOV residue was determined by assuming the MOV residue to be composed of 85% metals (determined by ICP-OES) with the remaining 15% being oxygen (Table 3).

Table 2 Values of TG operating parameters

Variable	Value
Reaction temperature (°C)	100–1000
Balance purge rate (mL/min)	10
Sample purge rate (mL/min)	90
Sample size (mg)	10
Heating rate (°C/min)	5
Reaction gas	N_2

Results and Discussion

Thermodynamic Predictions

Thermodynamic models based on the calculation of the variation of Gibbs free energy ($\Delta G°$) can point out which reactions are more likely to take place under the conditions in a thermal decomposition or carbothermal reduction. Thermodynamic calculations do not model exactly the real processes, since simplified assumptions have to be made (ideal thermodynamic conditions, homogeneous distribution of the elements, chemical equilibrium, etc.), which can be far from reality in some systems Nevertheless, thermodynamic models can be powerful tools for understanding chemical behavior during thermal and reducing conditions.

Thermodynamic analysis was done over a temperature range between 100 and 1000 °C. The possible reactions occurring during thermal treatment of Sb_2O_3, Bi_2O_3, and ZnO are shown as a function of equilibrium composition in Fig. 2a. Sb_2O_3(s) starts to equilibrate with Sb_2O_3(l) near 630 °C, the predicted melting temperature of Sb_2O_3. It is also seen that Sb_4O_6(g) forms around the same temperature. Bi_2O_3 is stable through the entire temperature range.

Table 3 Molar ratio of C/O used for carbothermal reduction

Compound	C/O ratio used
Antimony oxide, Sb_2O_3	2
	4
Bismuth oxide, Bi_2O_3	2
	4
Zinc oxide, ZnO	2
	4
MOV residue	1.4
	2.2
	8.6

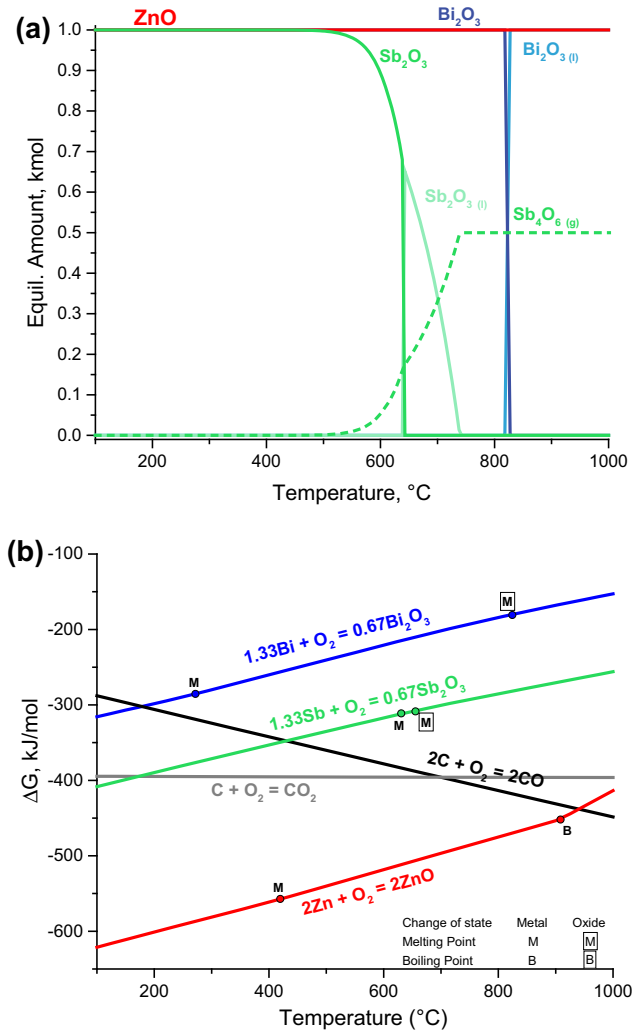

Fig. 2 **a** Equilibrium composition for heat-treated Sb_2O_3, Bi_2O_3, and ZnO in inert atmosphere. **b** Ellingham diagram for oxidation of metals. $P = 1$ atm (Color figure online)

Melting of Bi_2O_3(s) occurs at 825 °C. A phase transformation from α-Bi_2O_3(s) to γ-Bi_2O_3(s) takes place at 730 °C but is not shown in Fig. 2a since these data were not available in the HSC database. However, the transition was reported to occur by Irtyugo et al. [25]. ZnO is stable in the temperature range shown in Fig. 2a.

An Ellingham diagram as shown in Fig. 2b was used to determine the variation of $\Delta G°$ (compound stability) with temperature for the oxidation of a series of metals. The lower the position of a metal's line in the Ellingham diagram, the greater the stability of its oxide. For instance, ZnO is more stable than Bi_2O_3. In general, the stability of metal oxides decreases with temperature. A reduced metal, whose Gibbs free energy of formation is lower on the diagram at a given temperature, will reduce an oxide whose free energy of formation is higher on the diagram. For example, metallic zinc can reduce Sb_2O_3 to metallic antimony, the zinc itself being oxidized to ZnO. Because the distance is greater between Bi_2O_3 and ZnO as compared to Sb_2O_3 and ZnO, Zn will be more effective as a reducing agent for Bi_2O_3.

The $\Delta G°$ of carbon dioxide (CO_2) is almost independent of temperature, while that of carbon monoxide (CO) has negative slope and intersects the CO_2 line near 700 °C. According to the Boudouard reaction (R1), carbon monoxide is the dominant oxide of carbon at higher temperatures (above 700 °C), and the higher the temperature the more effective CO is as a reducing agent.

$$2CO \leftrightarrow CO_2 + C \qquad (R1)$$

It can be expected from thermodynamic calculations that Sb_2O_3 will melt near 630 °C and the formation of Sb_4O_6(g) upon further heating is also anticipated. During carbothermal reduction of Sb_2O_3, reduction of Sb_2O_3 is predicted to occur above 400 °C, while reduction of Bi_2O_3 occurs near 200 °C and volatilization of ZnO at 900 °C with equilibrium between CO and ZnO occurring at 940 °C.

Sb_2O_3

Sb_2O_3 is white, has a melting point of 656 °C, and volatilizes thereafter [22]. There are two crystal structures of Sb_2O_3: the cubic (senarmontite) consisting of Sb_4O_6 units [26] and orthorhombic (valentinite) having a layered structure [27]. Typically, commercial samples of Sb_2O_3 contain both cubic and orthorhombic forms of Sb_2O_3 [28]. The Sb_2O_3 used here was shown to be cubic by XRD. The structure of antimony(III) oxide in the vapor phase has been shown to be discrete Sb_4O_6 molecules of Sb_4O_6 which dissociate into SbO_3 trigonal pyramidal units at high temperatures [29]. Heating causes the cubic phase to change to the denser (5.20–5.79 g/mL) orthorhombic form followed by a structural change to the polymeric form $[Sb_2O_3]_n$ [29].

$$Sb_4O_6(\text{cubic}) \overset{570°C}{\rightleftharpoons} [Sb_2O_3]_n(\text{orthorhombic}) \rightleftharpoons Sb_4O_6(l) \rightleftharpoons Sb_4O_6(g)$$

The effect of mass loss as a function of heating rate on Sb_2O_3 is shown in Fig. 3a and the rate of mass loss is given in the derivative thermogravimetric (DTG) curve shown in Fig. 3b. It has been reported that the first thermal effect to occur upon heating senarmontite is the onset of sublimation occurring at approximately 500 °C [30, 31]. This is shown in Fig. 3a. From the DTG curve, the peak volatilization temperature was determined to be 644 °C at a heating rate of 20 °C/min and decreased with slower heating rates. The temperature range in which Sb_2O_3 was sublimated was 500–650 °C. Thermal decomposition curves indicate that Sb_2O_3 sublimated in one step from Sb_2O_3(s) to Sb_4O_6(g); this is seen in Fig. 3a where mass loss curves are smooth

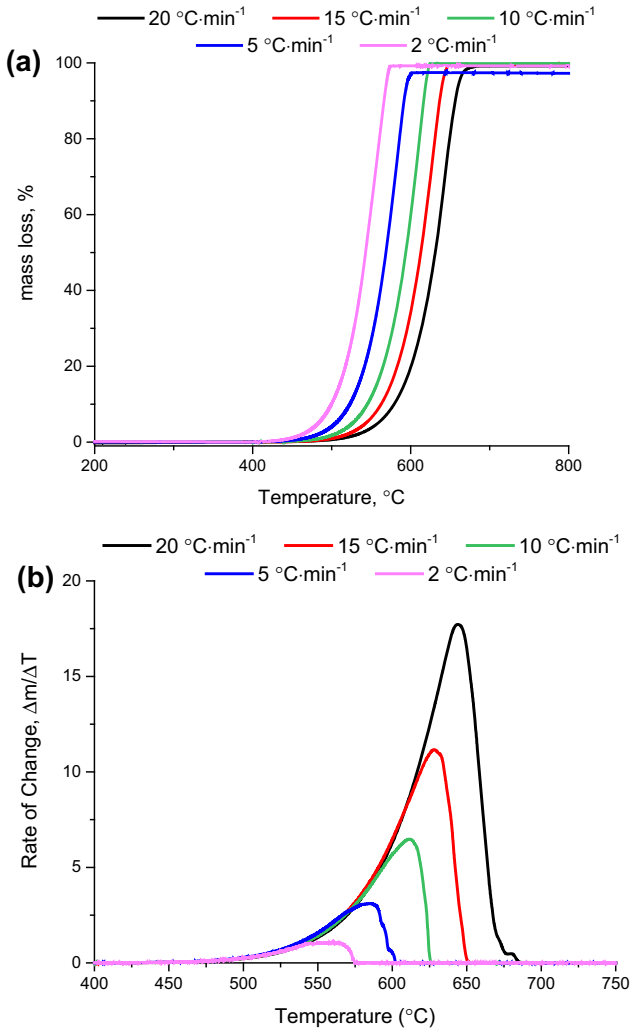

Fig. 3 **a** Effect of heating rate on direct thermal decomposition of Sb_2O_3 in nitrogen atmosphere. The heating rates used are 20, 15, 10, and 5 °C/min. **b** DTG curve (Color figure online)

and continuous. Similar results were reported by Orman et al. [32] for cubic Sb_2O_3 decomposition.

Generally, the oxides of more noble metals can be converted directly by thermal decomposition to metal from their oxides in the presence of a reducing agent, such as carbon. Antimony oxides can be reduced with charcoal in a reverberatory furnace at temperatures near 1200 °C. The reaction proceeds according to reaction R2–R3 [20].

$$Sb_2O_3 + 3C \rightarrow 2Sb + 3CO \quad (R2)$$

$$3CO_2 + 3C \rightarrow 6CO \quad (R3)$$

The thermograms for carbothermal reduction of antimony oxide are shown in Fig. 4. The addition of carbon to antimony oxide does nothing to lower the volatilization temperature. This is evident where each curve overlaps and has the same onset temperature for Sb_2O_3 volatilization. Complete volatilization of Sb_2O_3 (with no Sb_2O_3/C

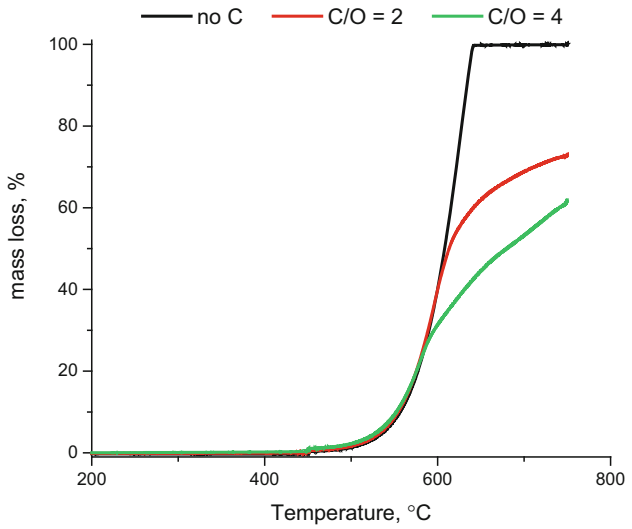

Fig. 4 Effect of molar ratio of C/O on mass loss of Sb_2O_3 during heating to 750 °C, isotherm for 10 min, heating rate 10 °C/min (Color figure online)

interaction) should result in 90 and 75% mass loss for C/O of 2 and 4, respectively. TGA results show that 73 and 62% of sample mass was lost when the C/O ratio was 2 and 4, respectively. From Fig. 4 it can be see that the rate of mass loss changes in the presence of carbon around 600 °C. The slower reaction kinetics could be due to the formation and then diffusion of Sb_4O_6 gas molecules through the sample. It could also be caused by carbothermal reduction of liquid or gaseous Sb_2O_3 which is predicted to occur near 430 °C from the Ellingham diagram shown in Fig. 2b. Antimony is less volatile than Sb_2O_3 and would therefore lower the rate of mass loss when compared to the pure Sb_2O_3 sample [22, 33]. However, no further analysis was performed on the remaining residue and therefore the presence of antimony metal could not be determined.

Bi_2O_3

Bi_2O_3 has a melting point of 820 °C [29] and is volatile at higher temperatures. As shown in Fig. 5, the black curve shows no mass loss of Bi_2O_3 below 980 °C and therefore no thermal decomposition occurred. The addition of carbon to bismuth oxide results in carbothermal reduction of Bi_2O_3 into a metallic Bi product [34]. Carbothermal reduction reactions depicted in Fig. 5 show Bi_2O_3 was reduced to metallic Bi at 596 °C, above which Bi started to volatilize. Mass balance calculations for carbothermal reduction of Bi_2O_3, to bismuth metal, predict a 15.6 and 13.8% mass loss for C/O of 2 and 4, respectively. Theoretical data are in good correlation with experimental data. Increasing the C/O molar ratio did not have any significant effect on the rate of carbothermal reduction.

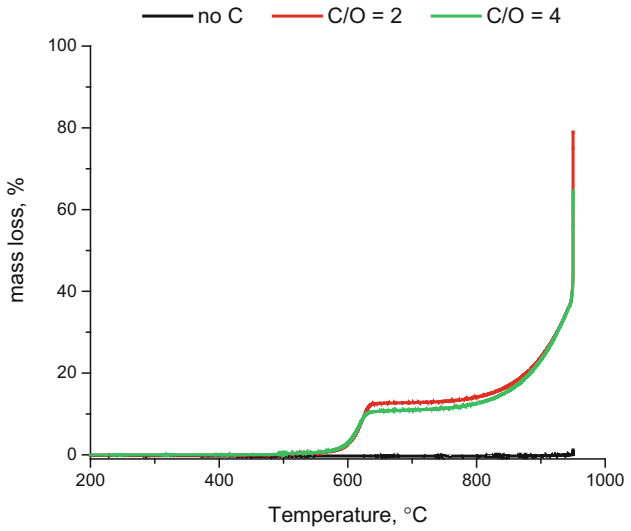

Fig. 5 Effect of molar ratio of C/O on mass loss of Bi_2O_3 during heating to 980 °C, heating rate 10 °C/min, 30 min isotherm at 980 °C for 30 min (Color figure online)

Inspection of the sample after TG experiments indicated that carbon was added in excess and parts of it remained unreacted in the crucible. Mass balance calculations indicate that 50% of the carbon in the C/O = 2 sample and 25% in the C/O = 4 sample was used. Metallic pieces of bismuth metal were also seen in the crucible.

Complete carbothermal reduction and Bi volatilization would yield a mass loss of 93% and 82% for C/O = 2 and 4, respectively. In these experiments, the samples were heated to 980 °C and held isothermally for 30 min. The TG curves indicate an 80% mass loss when the C/O = 2 and 65% mass loss for C/O = 4. The difference between theoretical and experimental results is explained by the kinetics of bismuth volatilization. It is possible that not all molten bismuth was volatilized before the end of the heating segment.

ZnO

It is well known that in high-temperature zinc production carbon is added to zinc oxide causing carbothermal reduction, yielding zinc. Carbothermal reduction of zinc oxide occurs according to reactions R4–R5 [34]. For ZnO to be continuously reduced, the equilibria in R4 and R5 must be satisfied [35]. Reduction with carbon is governed by the chemical equilibria and reduction kinetics.

$$ZnO + CO \rightarrow Zn(g) + CO_2 \quad (R4)$$

$$CO_2 + C \rightarrow 2CO \quad (R5)$$

For zinc oxide, it is well documented that the melting point is 1975 °C and it does not thermally decompose below this temperature [22]. Carbothermal reduction of ZnO producing Zn(g) and CO_2(g) has been shown to occur at 907 °C [36, 37]. TG curves of mass loss as a function of C/O ratio are shown in Fig. 6. In the absence of carbon, zinc oxide showed no weight loss up to 950 °C. The addition of carbon with a C/O molar ratio of 2 and 4 resulted in carbothermal reduction of zinc starting near 800 °C. The boiling point of Zn is 907 °C under a pressure of 1 bar and evaporation starts when the partial pressure of vapor of the zinc is lower than the equilibrium vapor pressure [22, 38]. As the temperature was increased, the rate of zinc reduction increased which has been seen in other reported in literature [37].

Volatilization of Sb_2O_3 occurred from 400 to 650 °C with the peak volatilization temperature of 644 °C at a heating rate of 20 °C/min. The addition of carbon had no effect on the Sb_2O_3 volatilization temperature because of the low temperature at which sublimation occurred. However, the volatilization rate was affected due to carbothermal reduction of a portion of the Sb_2O_3 and subsequent volatilization of antimony. For Bi_2O_3, the addition of carbon resulted in a 10–15% mass loss near 600 °C. The reaction thought to occur at this temperature is transition of Bi_2O_3 to molten Bi. The melting temperature of Bi metal is 217 °C [29]. Another mass loss with onset near 875 °C is due to volatilization of Bi. It is known that bismuth metal is volatile at high temperatures. However, when in the presence of other metals, bismuth will not volatilize at high temperatures; rather it will alloy with the metals. Carbothermal reduction of ZnO to Zn(g) occurred just above 901 °C in these experiments. This is a very well-known reaction and the results obtained here correlate well with literature.

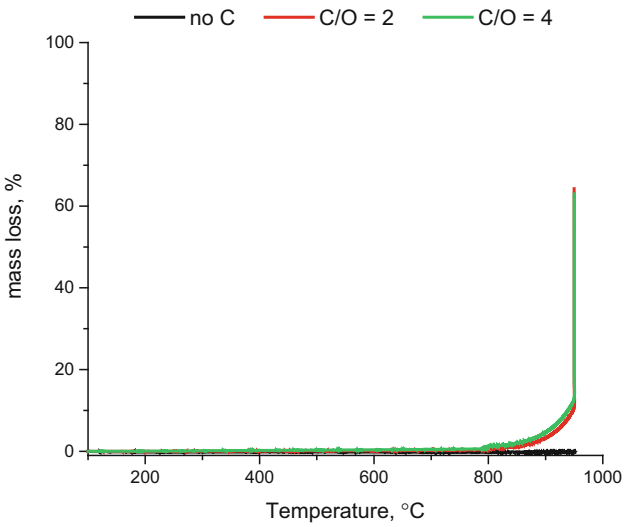

Fig. 6 Effect of molar ratio of C/O on mass loss of ZnO during heating to 950 °C, isotherm for 30 min, and heating rate 10 °C/min (Color figure online)

Thermal treatment of the simple metal oxides suggests that sublimated antimony oxide could be separated from a mixture of Sb_2O_3, Bi_2O_3, and ZnO by heating to 650 °C and collected by distillation. The addition of carbon causes the volatilization of Sb_2O_3 and the reduction of Bi_2O_3 to occur at nearly the same temperature. If separation of bismuth and zinc was of interest, then after antimony volatilization, carbon could be added to lower the reduction temperature for their recovery.

MOV and MOV Residue

Prior to pretreatment, the MOV consisted of three main phases: firstly, the bulk zinc oxide phase, which accounted for nearly 90% of the MOV; secondly, the bismuth oxide phase, found in the region between the zinc oxide grains; and lastly the phase containing antimony compounds such as spinel ($Zn_7Sb_2O_{12}$) and pyrochlore ($Zn_2Bi_3Sb_3O_{14}$). The antimony compounds are found within the bismuth oxide phase. Cobalt, manganese, and nickel are also present in the MOV most likely substituted into the spinel lattice. Work by Wong [39] determined that the octahedral crystal of the $Zn_7Sb_2O_{12}$ spinel was doped with Mn and Co when Mn and Co were present during sintering. XRD analysis of the residue supports this conclusion where peaks were seen for Zn–Co–Sb–O and Zn–Ni–Sb–O compounds.

It was shown in previous research that leaching-pulverized MOVs with a pH 3 sulfuric acid solution resulted in selective leaching of the zinc oxide phase, leaving the bismuth- and antimony-containing phases in the MOV residue [15]. XRD analysis of the residue showed the presence of Bi_2O_3, α-$Zn_7Sb_2O_{12}$, β-$Zn_{2.33}Sb_{0.67}O_4$, and $Zn_2Bi_3Sb_3O_{14}$. There are two polymorphous forms of the $Zn_7Sb_2O_{12}$ compound. The cubic α-$Zn_7Sb_2O_{12}$ having a crystal structure of the inverse spinel and orthorhombic β-$Zn_{2.33}Sb_{0.67}O_4$, in which the crystal structure is not understood. Mn, Ni, and Co are substituted in the spinel lattice.

Since antimony is not found as Sb_2O_3 but within the spinel and pyrochlore compounds, the fate of antimony during thermal treatment of the MOV residue is not clear. The spinel compound has been reported to be stable up to 1350 °C [40]. Filipek et al. have suggested thermal decomposition of spinel occurs according to reaction R6.

$$2\alpha - Zn_7Sb_2O_{12(s)} \rightleftharpoons 14ZnO_{(s)} + Sb_4O_{6(g)} + 2O_{2(g)} \quad \text{(R6)}$$

Thermal decomposition of the MOV residue in the absence of carbon resulted in less than 5% mass loss. The addition of carbon to the MOV residue had a large effect on the mass loss as seen in Fig. 7. For all samples containing carbon, there are four inflections indicating several stages

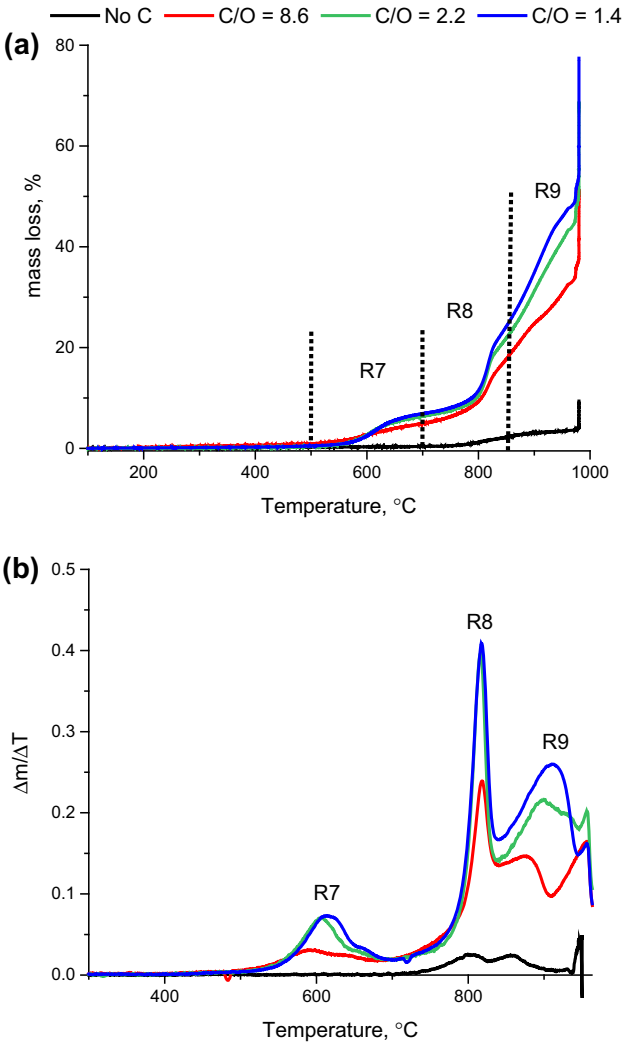

Fig. 7 **a** Effect of C/O molar ratio on mass loss of MOV residue during heating to 980 °C, heating rate 10 °C/min. **b** Derivative curve for mass loss as a function of temperature (Color figure online)

of decomposition occurring in the MOV residue-carbon samples. Mass loss increased with temperature due to thermal decomposition, representing the mass of volatile matter removed from the sample. The decomposition regions are labeled in Fig. 7 and correspond to the decomposition reactions given in R7–R9. The decomposition mechanisms proposed are based on this research, literature data, and mass balance calculations.

$$500-700\,^{\circ}C \quad Bi_2O_{3(s)} + 3C \rightleftharpoons 2Bi_{(s)} + 3CO_{(g)} \quad \text{(R7)}$$

$$700-850\,^{\circ}C \quad 2Zn_7Sb_2O_{12(s)} + 4C \rightleftharpoons 14ZnO_{(s)} + Sb_4O_{6(g)} + 4CO_{(g)} \quad \text{(R8)}$$

$$\sim 900\,^{\circ}C \quad ZnO_{(s)} + C \rightleftharpoons Zn_{(g)} + CO_{(g)} \quad \text{(R9)}$$

The first reaction is the loss of oxygen forming liquid Bi (R7) occurring at 600 °C. In the presence of carbon, R8 has

Table 4 Theoretical mass loss (in wt%) from mass balance calculations and experimental mass loss for reactions R7–R9

Reaction	Theoretical			Experimental		
	C/O = 8.6	C/O = 2.2	C/O = 1.4	C/O = 8.6	C/O = 2.2	C/O = 1.4
R7	2.5	4.0	4.3	4.6	6.3	6.8
R8	13.2	21.2	22.8	12.7	15.5	17.3
R9	24.9	39.9	42.9	34.2	46.9	54.2
Subtotal	40.7	65.1	70.0	51.5	68.7	78.3
Co, Ni, Mn	2.6	4.2	4.5			
Bi	12.3	19.7	21.2			
C	44.9	11.8	5.1			
Total	109.1	103.0	102.3			

been proposed as the decomposition mechanism for α-$Zn_7Sb_2O_{12}$. Complete decomposition of $Zn_7Sb_2O_{12}$ would result in a theoretical mass loss of approximately 65.7% when the C/O = 1.4. The experimental mass loss between 700 and 980 °C was 71.5%, indicating that the decomposition of spinel occurs in this range. In addition it is possible that a portion of the Bi was also volatilized in this range explaining why the experimental mass loss is higher than theoretical mass loss.

Since it is known that ZnO decomposed according to R9 near 900 °C, the reaction near 800 °C is assumed to be volatilization of Sb_4O_6. The theoretical weight loss is 22.8%, while the experimental weight loss for Sb_4O_6 and CO was 17.3%. The difference in values is expected due to multiple reactions occurring near 900 °C. This is depicted in Fig. 7b, where the derivative curve does not return to baseline before the ZnO reduction reaction (R9) begins.

The calculated and experimentally determined weight losses for reactions R7–R9 are given in Table 4. Theoretical weight loss calculations were made using the following assumptions and the composition of the MOV residue given in Table 1:

1. All Bi in the sample is in the form of Bi_2O_3.
2. All Sb in the sample is in the form $Zn_7Sb_2O_{12}$. This also accounts for 97% of the Zn in the sample.
3. Liquid Bi, Co, Ni, Mn remain as a solid in the residue.
4. The C used is calculated from reactions R7–R9.

There are small deviations when comparing theoretical and experimental data. From the derivative curves shown in Fig. 7b, it is seen that decomposition R8 is not complete before decomposition R9 begins. Multiple reactions occur simultaneously; therefore the experimental mass loss from an explicit decomposition reaction should only be viewed as an estimate. Simultaneous reactions will cause deviation between theoretical and experimental data. Also, the volatilization of Bi could not be accounted for in the theoretical calculations and therefore the mass loss will always be slightly lower than the experimentally obtained data.

Metals such as cobalt, nickel, and manganese make up less than 5% of the MOV residue and are not accounted for in the mass balance calculations. Since they are substituted into the spinel lattice they are believed to remain after decomposition and volatilization of zinc and antimony. As shown in Table 4, Subtotal refers to total mass loss from reaction R7–R9 while Total accounts for the other metals (Co, Ni, Mn), liquid bismuth, and unreacted carbon. The Bi, unreacted carbon, and other metal remains are assumed to remain in the solid phase and do not contribute to mass loss.

It has been reported once that molten bismuth will volatilize at high temperatures. This is seen in Fig. 5 when reducing pure Bi_2O_3. The weight loss curve above 700 °C is smooth with no sharp inflection points, indicating the slow kinetics of bismuth volatilization. In the presence of other metals, bismuth tends to be less volatile. It can be concluded that some of the bismuth remained in the sample and some was volatilized. This would also explain the deviation between theoretical and experimental mass loss.

Conclusions

The MOV under investigation in this study was composed of sintered metal oxides of zinc, antimony (3.2 mol%), bismuth (2.3 mol%), cobalt (< 1 mol%), nickel (< 1 mol%), and manganese (< 1 mol%) [15, 16]. The microstructure of the MOV contains three phases: the most dominant phase is that of the zinc oxide grains; the bismuth-rich phase encompasses the zinc oxide grains; and the antimony-rich phase is located within the bismuth oxide phase.

When recycling low concentration metals from waste, pretreatment is often needed. Pulverized (< 65 μm) MOV was leached at pH 4 using H_2SO_4 yielding a pure zinc sulfate solution and an antimony-rich residue. XRD analysis showed antimony compounds such as $Zn_7Sb_2O_{12}$, $Zn_{2.33}Sb_{0.67}O_4$, and $Zn_2Bi_3Sb_3O_{14}$ as well as Bi_2O_3 to be present in the insoluble MOV residue.

In this work, thermogravimetry was used to investigate the weight loss and rate of weight change of simple metal oxides (Sb_2O_3, Bi_2O_3, ZnO) as well as those of the MOV leaching residue as a function of temperature in inert and reducing conditions. Simple metal oxides were used as a reference to help predict the behavior of the sintered metal oxide compounds ($Zn_7Sb_2O_{12}$, $Zn_{2.33}Sb_{0.67}O_4$, and $Zn_2Bi_3Sb_3O_{14}$) present in the MOV residue.

The thermal treatment of the simple metal oxides suggested that sublimated antimony oxide could be separated from a mixture of Sb_2O_3, Bi_2O_3, and ZnO by heating to 650 °C and collected by distillation. The addition of carbon causes volatilization and reduction of Sb_2O_3 followed by subsequent Sb volatilization at a slower rate than for Sb_2O_3. Carbothermal reduction of Bi_2O_3 and subsequent volatilization of Bi(l) occurred at nearly the same temperature. For the separation of bismuth and zinc, once antimony was volatilized, carbon could be added to lower the reduction temperature for their recovery.

It was not known whether the spinel $Zn_7Sb_2O_{12}$ is found in the cubic, orthorhombic, or a mixture of both forms in the MOV residue. Also, some antimony may be found in the pyrochlore $Zn_2Sb_3Bi_3O_{14}$ phase. For this work, all mass balance calculations were made assuming antimony was in the $Zn_7Sb_2O_{12}$ compound. This could give rise to small deviations in mass balance calculations. The major part of theoretical deviations are most likely due to Bi vaporization.

Others have suggested thermal decomposition of spinel occurs near 1350 °C yielding ZnO and Sb_4O_6. Therefore, spinel decomposition was not expected to occur below 1350 °C without the addition of carbon. It was seen that decomposition of the MOV residue in the absence of carbon resulted in less than 5% mass loss. The addition of carbon to the MOV residue had a large effect on the mass loss. The first reaction, occurring around 600 °C, was the reduction of Bi_2O_3 from the MOV, while near 800 °C volatilization of Sb_4O_6 occurred. The theoretical weight loss was 22.8%, while the experimental weight loss for Sb_4O_6 and CO_2 was 17.3%. At temperatures above 900 °C, zinc was volatilized and reduced.

Thermal treatment and carbothermal reduction of Bi_2O_3 showed that once reduced, Bi metal was slowly volatilized. This is also believed to occur during carbothermal reduction of the MOV residue. Therefore, antimony can be collected from the vapor phase at 800 °C with small amount of bismuth present. Further separation of antimony and bismuth was not investigated here.

Acknowledgements The authors of this work would like to thank their colleagues Volkmar Frick and Mikael Karlsson for their contributions to this work. Funding was provided by Chalmers Area of Advance Production, which is gratefully acknowledged.

Compliance with Ethical Standards

Conflict of interest The authors declare that they have no conflict of interest.

References

1. CRM-EU (Critical Raw Materials for the EU) (2010) Report of the Ad hoc Working Group on defining critical raw materials. http://ec.europa.eu/enterprise/policies/rawmaterials/documents/index_en.htm
2. Guberman DE (2017) Mineral information antimony. In: USGS (ed.) US Geological Survey, Mineral Commodity Summaries, Washington, DC
3. Guberman DE (2014) US Geological Survey, Mineral Commodity Summaries, Washington, DC, p 196
4. Graedel TE, Reck BK (2014) Chapter 3—recycling in context. In: Worrell E, Reuter MA (eds) Handbook of recycling. Elsevier, Boston, pp 17–26
5. Rombach E, Friedrich B (2014) Chapter 10—recycling of rare metals. In: Worrell E, Reuter MA (eds) Handbook of recycling. Elsevier, Boston, pp 125–150
6. Nakamura K, Kinoshita S, Takatsuki H (1996) The origin and behavior of lead, cadmium and antimony in MSW incinerator. Waste Manag 16(5):509–517
7. Paoletti F, Sirini P, Seifert H, Vehlow J (2001) Fate of antimony in municipal solid waste incineration. Chemosphere 42(5–7):533–543
8. van Velzen D, Langenkamp H, Herb G (1998) Antimony, its sources, applications and flow paths into urban and industrial waste: a review. Waste Manag Res 16(1):32–40
9. Takaoka M, Yamamoto T, Tanaka T, Takeda N, Oshita K, Uruga T (2005) Direct speciation of lead, zinc and antimony in fly ash from waste treatment facilities by XAFS spectroscopy. Phys Scr 2005(T115):943
10. Wang L, Chen Q, Jamro IA, Li R, Li Y, Li S, Luan J (2016) Geochemical modeling and assessment of leaching from carbonated municipal solid waste incinerator (MSWI) fly ash. Environ Sci Pollut Res 23(12):12107–12119
11. Johansson I, Sahlin E, Bahr BV, Björkmalm J, Olsson JT (2013) Kritiska metaller i svenska avfallsaskor. In: The content of critical elements in residues from Swedish waste-to-energy plants. SP Sveriges Tekniska Forskningsinstitut, Waste Refinery, Borås
12. Johnson CA, Moench H, Wersin P, Kugler P, Wenger C (2005) Solubility of antimony and other elements in samples taken from shooting ranges. J Environ Qual 34(1):248–254
13. Levinson LM, Philipp HR (1986) Zinc oxide varistors—a review. Ceramic Bulletin 65(4):639–646
14. Hultgren H (2014) Varistor material information. Personal communication
15. Gutknecht T, Gustafsson AMK, Forsgren C, Ekberg C, Steenari B-M (2017) Investigations into recycling zinc from used metal oxide varistors via ph selective leaching: characterization, leaching, and residue analysis. Sci World J 2015:11

16. Gutknecht T, Colombus Y, Steenari B-M (2017) Recycling zinc from metal oxide varistors through leaching and cementation of cobalt and nickel. J Sustain Metall 3(2):239–250
17. Bernik S, Maček S, Bui A (2004) The characteristics of ZnO–Bi_2O_3-based varistor ceramics doped with Y_2O_3 and varying amounts of Sb_2O_3. J Eur Ceram Soc 24(6):1195–1198
18. Arefin ML, Raether F, Dolejš D, Klimera A (2009) Phase formation during liquid phase sintering of ZnO ceramics. Ceram Int 35(8):3313–3320
19. Kim JC, Goo E (1989) Morphology and formation mechanism of the pyrochlore phase in ZnO varistor materials. J Mater Sci 24(1):76–82
20. Anderson CG (2012) The metallurgy of antimony. Chem Erde Geochem 72(Supplement 4):3–8
21. Carlin JF (2000) Antimony recycling in the United States in 2000. In: Flow studies for recycling metal commodities in the United States. U.S. Department of the Interior, U.S. Geological Survey, Washington, DC
22. Weast RC (ed) (1976) Handbook of chemistry and physics, 57th edn. CRC Press, Cleveland
23. JCPDS (2010) Joint committee of powder diffraction standards. In: JCPDS-ICCD 2010, Philadelphia
24. Gordon RB, Graedel TE, Bertram M, Fuse K, Lifset R, Rechberger H, Spatari S (2003) The characterization of technological zinc cycles. Resour Conserv Recycl 39(2):107–135
25. Irtyugo LA, Belousova NV, Denisov VM, Denisova LT, Kirik SD, Chumilina LG (2012) High-temperature heat capacity of bismuth oxide and bismuth-zinc double oxide with the sillenite structure. J Sib Fed Univ 2:125–130
26. Svensson C (1975) Refinement of the crystal structure of cubic antimony trioxide, Sb_2O_3. Acta Crystallogr B 31(8):2016–2018
27. Svensson C (1974) The crystal structure of orthorhombic antimony trioxide, Sb_2O_3. Acta Crystallogr B 30(2):458–461
28. Golunski SE, Jackson D (1989) Antimony oxides: a guide to phase changes during catalyst preparation. Appl Catal 48(1):123–135
29. Norman NC (1998) Chemistry of arsenic, antimony and bismuth. Blackie Academic & Professional, London
30. Cody CA, DiCarlo L, Darlington RK (1979) Vibrational and thermal study of antimony oxides. Inorg Chem 18(6):1572–1576
31. Golunski SE, Nevell TG, Pope MI (1981) Thermal stability and phase transitions of the oxides of antimony. Thermochim Acta 51(2–3):153–168
32. Orman RG, Holland D (2007) Thermal phase transitions in antimony (III) oxides. J Solid State Chem 180(9):2587–2596
33. Paoletti F, Seifert H, Vehlow J, Sirini P (2000) Oxyanions forming elements in waste combustion—partitioning of antimony. Waste Manag Res 18(2):141–150
34. Rosenqvist T (1974) Reduction of metal oxides. In: Clark BJ (ed) Principles of extractive metallurgy. McGraw-Hill, New York, pp 264–298
35. Rosenqvist T (1974) Volatile metals. In: Clark BJ (ed) Principles of extractive metallurgy. McGraw-Hill, New York, pp 299–321
36. Guger CE, Manning FS (1971) Kinetics of zinc oxide reduction with carbon monoxide. Metall Mater Trans B 2(11):3083–3090
37. Hong L, Sohn HY, Sano M (2003) Kinetics of carbothermic reduction of magnesia and zinc oxide by thermogravimetric analysis technique. Scand J Metall 32(3):171–176
38. Ebin B, Petranikova M, Steenari B-M, Ekberg C (2016) Production of zinc and manganese oxide particles by pyrolysis of alkaline and Zn–C battery waste. Waste Manag 51:157–167
39. Wong J (1975) Microstructure and phase transformation in a highly non-Ohmic metal oxide varistor ceramic. J Appl Phys 46(4):1653–1659
40. Filipek E, Dąbrowska G (2008) Unknown thermal properties of $ZnSb_2O_6$ and $Zn7Sb_2O_{12}$ compounds. J Therm Anal Calorim 94(1):195–201